Consistent Device Simulation Model Describing Perovskite Solar Cells in Steady-State, Transient, and Frequency Domain

Martin T. Neukom,[†,‡,§] Andreas Schiller,[*,†,‡] Simon Züfle,[†,‡] Evelyne Knapp,[†] Jorge Ávila,[∥] Daniel Pérez-del-Rey,[∥] Chris Dreessen,[∥] Kassio Zanoni,[∥] Michele Sessolo,[∥] Henk J. Bolink,[∥] and Beat Ruhstaller[†,‡]

[†]Institute of Computational Physics, Zurich University of Applied Sciences, Wildbachstr. 21, 8401 Winterthur, Switzerland

[‡]Fluxim AG, Loft 313, Katharina-Sulzer-Platz 2, 8400 Winterthur, Switzerland

[§]Institute of Physics, University of Augsburg, 86135 Augsburg, Germany

[∥]Instituto de Ciencia Molecular, Universidad de Valencia, C/J. Beltrán 2, 46980 Paterna, Spain

Ⓢ *Supporting Information*
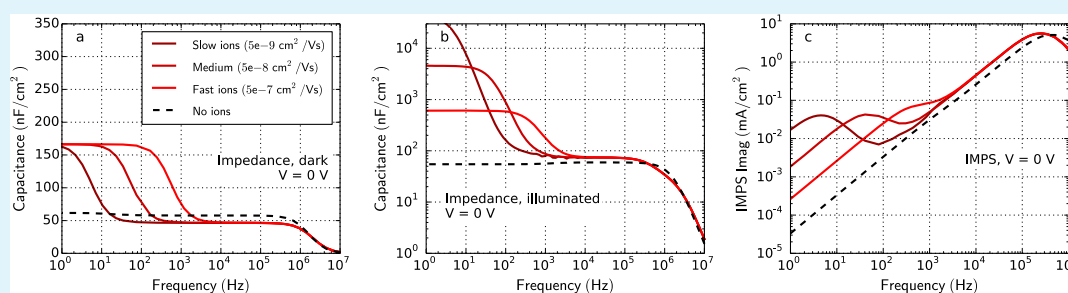
ABSTRACT: A variety of experiments on vacuum-deposited methylammonium lead iodide perovskite solar cells are presented, including *IV* curves with different scan rates, light intensity-dependent open-circuit voltage, impedance spectra, intensity-modulated photocurrent spectra, transient photocurrents, and transient voltage step responses. All these experimental data sets are successfully reproduced by a charge drift-diffusion simulation model incorporating mobile ions and charge traps using a single set of parameters. While previous modeling studies focused on a single experimental technique, we combine steady-state, transient, and frequency-domain simulations and measurements. Our study is an important step toward quantitative simulation of perovskite solar cells, leading to a deeper understanding of the physical effects in these materials. The analysis of the transient current upon voltage turn-on in the dark reveals that the charge injection properties of the interfaces are triggered by the accumulation of mobile ionic defects. We show that the current rise of voltage step experiments allow for conclusions about the recombination at the interface. Whether one or two mobile ionic species are used in the model has only a minor influence on the observed effects. A delayed current rise observed upon reversing the bias from +3 to −3 V in the dark cannot be reproduced yet by our drift-diffusion model. We speculate that a reversible chemical reaction of mobile ions with the contact material may be the cause of this effect, thus requiring a future model extension. A parameter variation is performed in order to understand the performance-limiting factors of the device under investigation.

KEYWORDS: perovskite solar cells, hysteresis, mobile ions, traps, impedance spectroscopy, IMPS, transient photo-current, drift-diffusion modeling

1. INTRODUCTION

Perovskite solar cells are promising candidates as top cells in tandem architectures with crystalline silicon or CIGS as bottom cell. A record efficiency of 26.7% has been demonstrated with methylammonium lead iodide (MAPI) perovskite on top of a silicon solar cell with the PERL structure.[1] Such perovskite-silicon tandem solar cells can potentially reach power conversion efficiencies beyond 30%.[2,3]

Organic−inorganic perovskites are electronic−ionic conductors, which is believed to be the reason for the observed *IV* curve hysteresis[4] and other intriguing effects like the extraordinarily high low-frequency capacitance under illumi-nation.[5] Thereby, iodine vacancies can migrate and lead to a screening of the electric field.[6−9] The exact physical operation mechanisms of perovskite solar cells remain, however, under debate.

The physical processes in these materials are often too complex to be understood by ad-hoc explanations or simple analytical formulas. Numerical simulations offer a deeper understanding of the underlying device physics. First charge

A
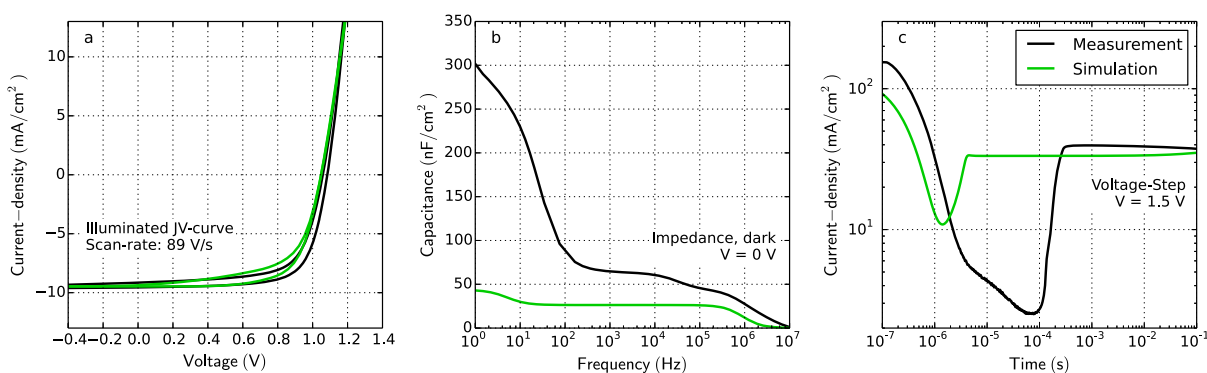
Figure 1. Example of simulation mismatch. Measurement (black) and simulation (green) of a planar perovskite solar cell. (a) JV curve with a ramp rate of 89 V/s. (b) Impedance spectroscopy in the dark. (c) Transient current as a response to a voltage step from 0 to 1.5 V at $t = 0$. Despite the agreement of simulation and measurement in the JV curve, they do not match impedance and voltage step experiments. Parameters extracted from JV curve fitting (a) are thus likely to be inaccurate.

drift-diffusion models incorporating mobile ions were presented by van Reenen,[10] Richardson,[11,12] and Calado.[13] In these models, the IV curve is simulated with a transient solver in forward and reverse directions, reproducing the observed IV curve hysteresis. Similar models were applied to simulate transient voltage steps,[14] open-circuit voltage transients,[15,16] transient photocurrents,[17] capacitance−voltage,[18] and impedance spectroscopy[18] as well as intensity-modulated photocurrent/photovoltage spectroscopy.[16]

Despite the success of these models in qualitatively reproducing the observed effects, it remains under debate whether mobile ions are sufficient to describe the working mechanism of perovskite solar cells. All models presented so far were usually applied to simulate a single experiment. Conclusions from only one experiment can be error-prone as we show in the following paragraph. We would like to note that these models also neglect RC effects, playing an important role in transient or frequency-domain experiments, hereby complicating the direct quantitative comparison of simulated and measured data. Therefore, this study, including series resistance, but mainly combining steady-state, transient, and frequency-domain experiments in the same model can not only confirm the above mentioned publications but also give additional insights with regard to the influence of mobile ions.

We measure the current−voltage (JV) curve, impedance spectroscopy in the dark, and a voltage step response of a MAPI perovskite solar cell (details on the cell structure in Section 2). Our numerical simulation model[19] is fitted to the transient JV curve. The hysteresis is well reproduced quantitatively as shown in Figure 1a. The same parameter set is now used to simulate the impedance spectroscopy and the voltage step results. As shown in Figure 1b,c, the simulation does not reproduce the measurement results well.

The parameter set describing the JV curve with hysteresis well does not match with the impedance spectroscopy results or the transient voltage step. The parameters are inaccurate and might be misinterpreted, although the JV curve is reproduced.

In the past, we have demonstrated parameter extraction of organic solar cells using numerical simulations.[20,21] By fitting numerical simulations to measurement results for several experimental techniques, the parameter correlation can be reduced significantly.[20] Moreover, we have shown that a rather simple drift-diffusion model with constant charge mobilities, discrete traps, and Ohmic contacts is sufficient to simulta-

neously reproduce JV curve, photo-CELIV, OCVD, TPC, capacitance−voltage, impedance, and intensity-modulated photocurrent spectroscopy (IMPS) data for a bulk-hetero-junction organic solar cell.[21]

In this publication, we present various measurements and simulations of a planar MAPI perovskite solar cell. Our simulation model incorporating mobile ions and charge traps is capable of describing the hysteresis of JV curves with varied scan rates, the dependence of the open-circuit voltage on the light intensity, transient photocurrent, impedance spectroscopy in the dark and under illumination, and IMPS. The main signatures observed in all these experimental techniques are reproduced by the simulation model using one single parameter set for all simulations.

To the best of our knowledge, this is the most comprehensive description of the device physics of perovskite solar cells up to now. We show that the major physical effects observed in perovskite solar cells can consistently be described by a device model incorporating inert mobile ions and traps. Based on our model, we investigate the influence of mobile ions, traps, and other parameters on the experimental results. In the last section, we show a parameter analysis to determine which factors limit the device performance.

2. METHODS

2.1. Experimental Methods. All experiments were performed with the all-in-one measurement platform Paios 4.0 from Fluxim.[22] All experiments were computer-controlled and sequentially performed with minimal delay in order to minimize cell degradation between two measurements. A white light-emitting diode (LED) (maximum intensity 500 W/cm²) was used as illumination source for all experiments. Eight nominally identical solar cells were characterized to test the reproducibility. The full data set of all measured curves is shown in the Supporting Information.

2.2. Numerical Methods. The simulation model used in this study is implemented in the simulation software Setfos 4.6 from Fluxim.[19] The charge generation profile within the MAPI layer is calculated by the transfer matrix method using wavelength-dependent complex refractive indices of all layers.

Drift-diffusion calculations are performed within the three layers $N^4,N^4,N^{4''},N^{4''}$-tetra([1,1'-biphenyl]-4-yl)-[1,1':4',1''-terphenyl]-4,4''-diamine (TaTm) (p-doped hole transport layer), MAPI, and C_{60} (n-doped electron transport layer) as shown in Figure 2. All model equations are shown in the Supporting Information. Two mobile ionic species (one positive one negative) of the same density are allowed to move inside the MAPI layers. The interfaces to TaTm and C_{60} are treated as ion-blocking. In the MAPI layer, 0.5 eV deep traps lead to
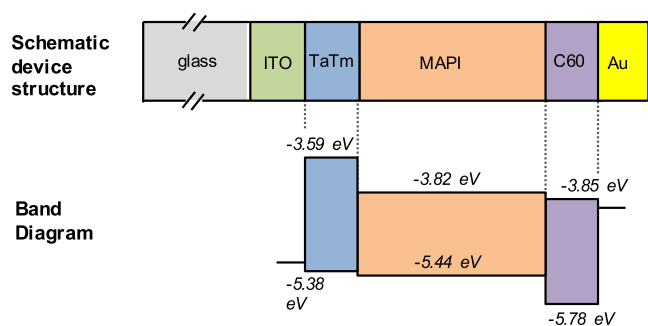
Figure 2. Device layout and band-diagram of the simulated device.

Shockley−Read−Hall (SRH) recombination. SRH recombination is necessary to reproduce the ideality factor of approximately 2 as observed in the light-intensity dependence of the open-circuit voltage. An external series resistance is considered in the simulation accounting for the combined effect of the internal measurement resistor (50 Ω) of the voltage source, the measurement resistor for current measurement (20 Ω), and further parasitic resistances as, for example, in the TCO.

The impedance spectra and the intensity-modulated photocurrent spectra are calculated from the Fourier transformation of a transient step response calculation as described by Ershov et al.[23]

We would like to stress the importance of taking the transport layers into account in such simulations. The voltage drop within the doped transport layers depends on their conductivity. The voltage drop inside the perovskite layer and the distribution of the mobile ions within the layer are consequently influenced by the contact layers.[24,25] The ion densities at the TaTm−MAPI and the MAPI−C$_{60}$

interfaces are much lower when contact layers are considered in the simulation.

We assume an equal density of iodine vacancies (cations) and methylammonium (MA) vacancies (anions) to be present in the device where the MA vacancies have a much lower mobility. We show in the Supporting Information that simulations with only iodine vacancies (cations) being mobile produce very similar results.

No direct interaction among ions is assumed and no interaction of ions with electrons, holes, or traps takes place. The position of the ions, however, influences the electric field inside the device and thereby the charge transport.

2.3. Device Fabrication. The solar cells were fully vacuum-processed using a previously reported protocol.[26] Briefly, the devices (scheme in Figure 2) were deposited in a p−i−n configuration onto indium tin oxide (ITO)-coated glass slides. TaTm was used as the hole transport material (HTM), either intrinsic or doped by co-sublimation with 2,2′-(perfluoronaphthalene-2,6-diylidene)-dimalononitrile (F$_6$-TCNNQ). The fullerene C$_{60}$ was used as the electron transport material (ETM), both intrinsic or doped by co-sublimation with N^1,N^4-bis(tri-*p*-tolylphosphoranylidene)benzene-1,4-diamine (PhIm). The MAPI perovskite films were prepared by dual source vacuum deposition of the two starting compounds, CH$_3$NH$_3$I and PbI$_2$, in a high vacuum chamber. The final device structure was ITO/TaTm:F$_6$-TCNNQ (40 nm)/TaTm (10 nm)/MAPI (500 nm)/C$_{60}$ (10 nm)/C$_{60}$:PhIm (40 nm)/Ag (100 nm). The active cell area is 0.065 cm^2.

3. RESULTS AND DISCUSSION

We perform measurements on perovskite solar cells, fabricated as described in the section Device Fabrication. To test the reproducibility 8, nominally identical devices were charac-
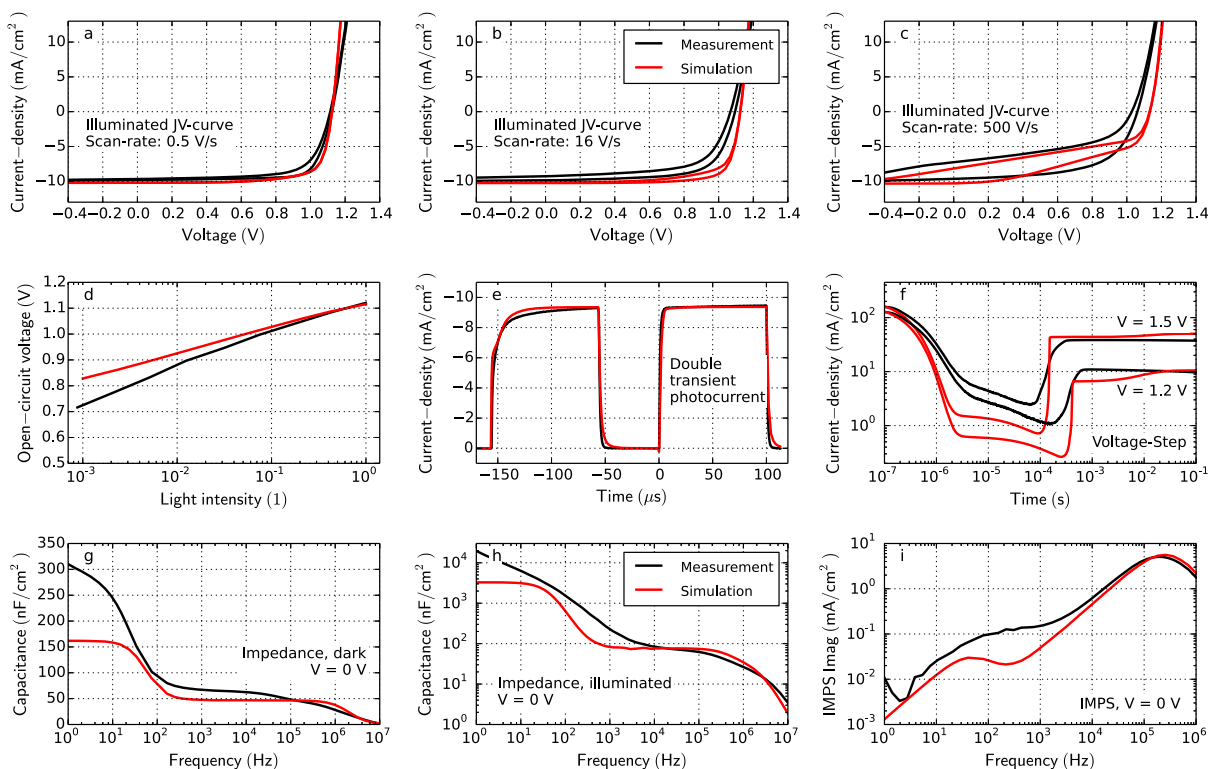
Figure 3. Measurement (black) and simulation (red) of the perovskite solar cell. (a−c) *IV* curves with hysteresis and varied scan rates. The device is illuminated with a white LED. The short-circuit current is therefore lower compared to the short-circuit current under AM1.5. (d) Dependence of the open-circuit voltage on the light intensity. (e) Photocurrent as a response to 2 subsequent light pulses. The first light pulse is from −160 to −50 μs. The second light pulse from 0 to 100 μs. (f) Transient current as a response to a voltage step in the dark in the log−log representation. (g) Impedance spectra in the dark in the capacitance−frequency representation. (h) Impedance spectra under illumination in the capacitance−frequency representation. (i) IMPS.
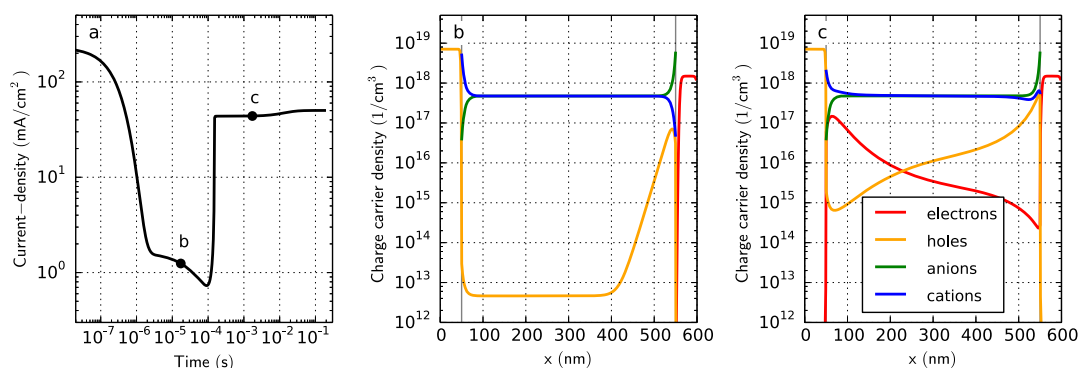
Figure 4. Simulation of a forward-bias voltage step from 0 to 1.5 V (a) Transient current. (b,c) Charge carrier density profiles of electrons, holes, anions and cations at two different time steps as marked in a. The HTM−perovskite and perovskite−ETM interfaces are located at 50 and 550 nm, respectively.
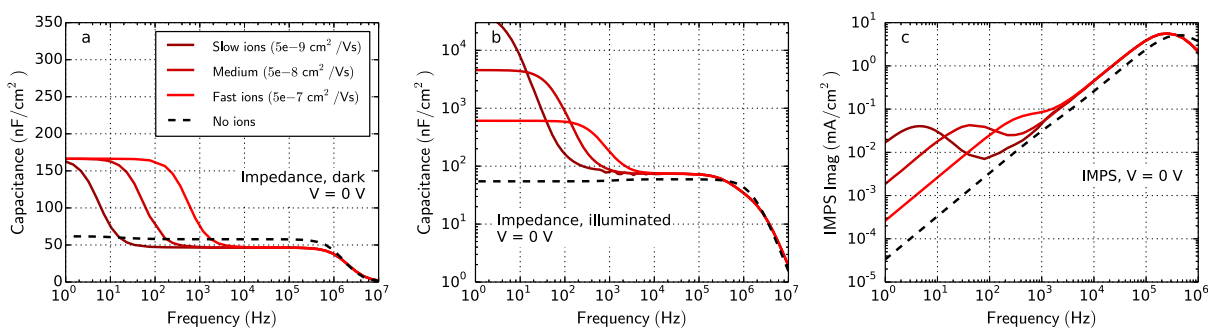
Figure 5. Simulation results with varied ion mobility and disabled ions (dashed line). (a) Impedance spectroscopy in the dark. (b) Impedance spectroscopy under illumination. (c) IMPS.

terized. The results of all cells are shown in the Supporting Information. For the sake of better readability, we show only one representative device in the manuscript.

The simulation model as described in the section Numerical Methods is applied to simulate the same characterization techniques as in the measurements. The parameters of the model are adjusted to reach an agreement between simulation and measurement.

Figure 3 shows measurement and simulation data for nine distinct experiments. In Figure 3a−c, JV curves measured by forward and reverse scan are shown. The scan rate is increased from (a) to (c). The short-circuit current of 10 mA/cm^2 is low because a white LED (500 W/cm^2) is used for the illumination instead of a sun simulator. With scan rates below 1 V/s, the hysteresis is very low. Only if very high scan rates up to 500 V/s are applied a pronounced hysteresis appears (Figure 3c). We simulate the same transient voltage ramp up and down to obtain an JV curve with hysteresis. At low scan rates, the hysteresis is small in the simulation as well as in the measurement (Figure 3a). With a higher scan rate, a pronounced hysteresis appears in the measurement and is well reproduced by the simulation. Here, we confirm that even hysteresis-free devices can have a hysteresis that is shifted to different time scales, consistent with the finding of Jacobs et al.[18]

The dependence of the open-circuit voltage on the light intensity is shown in Figure 3d. Its ideality $n_{id} = q/(k \times T) \times dV_{oc}/d(\ln(L))$ is clearly above 1.0, indicating dominant SRH recombination.[21,27,28] In the simulation, an ideality factor higher than 1.0 is only achievable with trap-assisted

recombination. The simulation reproduces the dependence of the open-circuit voltage on the light intensity.

Figure 3e shows the transient current response to two subsequent short light pulses. The measured current rise of the first pulse is significantly slower than the current rise of the second pulse. This behavior is reproduced very well by the simulation using traps. During the first light pulse, traps are being filled. In the subsequent pulse, the traps are already filled, and therefore, the current rise is faster. If the delay time between the two pulses is increased to milliseconds, the first and the second current rise are identical again. In this case, all trapped charges are released during the delay time. Therefore, the double light pulse measurement is well suited to study trapping in perovskite solar cells. Because of the short pulse length of 100 μs, this experiment is not sensitive to ion motion or accumulation (as long as the waiting time in the dark before the experiment is long enough).

In Figure 3f, the transient current as a response to a voltage step is shown. O'Kane et al. presented transient voltage step simulations on perovskite devices.[14] We use higher voltage steps than O'Kane which allows us to study charge injection as we detail in the following.

The current peak before 1 μs is the charging current of the device capacitance. Afterward, the current is small and then increases steeply at around 100 μs. To illustrate the origin of this effect, we plot the spatial charge carrier density profiles in Figure 4. The device is preconditioned at 0 V where the built-in voltage drives the cations (assumed to be iodine vacancies) to the hole contact layer. A few microseconds after the voltage step to 1.5 V is applied, the ions are still at their steady-state position (Figure 4b). The accumulated cations hinder hole

Table 1. Layer-Dependent Simulation Parameters Used for All Simulations in Figures 3−5

parameter	HTM, TaTm	MAPI	ETM, C_{60}
thickness	50 nm (measured)	500 nm (measured)	50 nm (measured)
electron mobility		0.2 cm^2/V s	8.9×10^{-4} cm^2/V s
hole mobility	1.5×10^{-3} cm^2/V s	0.1 cm^2/V s	
recombination constant		1×10^{-10} cm^3/s	
relative permittivity	3 (literature[34])	35 (literature[35])	3.9 (literature[34])
HOMO energy	5.38 eV	5.44 eV	5.77 eV
LUMO energy	3.59 eV	3.82 eV	3.85 eV
electron trap density		1.2×10^{16} $1/cm^3$	
electron trap depth		0.5 eV (literature[36])	
electron trap electron capture rate		3×10^{-10} cm^3/s	
electron trap hole capture rate		3×10^{-12} cm^3/s	
n-doping density			1.5×10^{18} $1/cm^3$
p-doping density	7×10^{18} $1/cm^3$		
mobile cation density		5×10^{17} $1/cm^3$	
mobile anion density		5×10^{17} $1/cm^3$	
cation mobility		5×10^{-8} cm^2/V s	
anion mobility		1×10^{-14} cm^2/V s	
effective density of states	1×10^{27} $1/m^3$	6×10^{25} $1/m^3$	1×10^{27} $1/m^3$

injection due to the strong electric field at the interface. After 1 ms, the cations have moved away from the interface (Figure 4c) enabling charge injection. Charges recombine in the bulk or at the opposite interface and a steady-state current flows.

In the simulation (Figures 3 and 4), the surface recombination is assumed to be very weak, corresponding to passivated, charge-selective contacts. Therefore, electrons can accumulate at the hole contact and holes can accumulate at the electron contact (Figure 4c). The steepness of the current rise after 100 μs (Figure 4a) is influenced by the surface recombination. A comparison of a device with high and with low surface recombination is presented in the Supporting Information.

We conclude that voltage step experiments are well suited to study the charge injection behavior of perovskite solar cells. As we show in the Supporting Information, a steep rise is an indication for low surface recombination.

Figure 3g shows the capacitance−frequency representation of an impedance measurement. The capacitance rise at low frequency (<100 Hz) is reproduced by the simulation. The transition frequency depends on the ion conductivity (ion density times the ion mobility). In Figure 5a, simulation results with varied ion mobility are shown. The transition frequency of the capacitance varies with the mobility. Varying the ion density has the same effect. If ions are disabled in the simulation, the capacitance remains low at low frequencies.

Figure 3h shows impedance spectroscopy data under illumination. Under illumination, the capacitance at low frequencies reaches extraordinarily high values, consistent with what has been reported in literature.[5] In these experiments, the word "capacitance" can be misleading. Moia and co-workers described the behavior as an "ionic-to-electronic current amplification".[29] The idea behind this is that the oscillating voltage moves the ions between the contacts. When ions are close to one contact, injection is enhanced, and if they are close to the other contact, injection is suppressed. An increased injection enables a large electron−hole current to flow in phase with the modulated ions. The mobile ions only open the door for electronic charges. Because the ion accumulation is out-of-phase with the voltage modulation, the electronic current is also out-of-phase and a

very high apparent capacitance is observed. The higher the bulk conductivity, the higher is the observed "capacitance". Hence, the observed "capacitance" increases with illumination. Our simulation reproduces this effect, and capacitance values of more than 1 μF/cm^2 are reached at 1 Hz. The same mechanism is also well-explained by Jacobs et al. using numerical simulation[18] and Pockett et al. using equivalent circuit modeling.[16] Furthermore, its relation to hysteresis and voltage step response was recently discussed by Ebadi et al.[30] The magnitude of the capacitance and the frequency of the onset depend on the ion mobility as shown in Figure 5b. Without mobile ions, the capacitance remains low.

Figure 3i shows IMPS data. In this technique, the light intensity is modulated and the current response is measured.[21,31,32] The peak of the imaginary part of the IMPS signal is often attributed to a charge transport time.[21] In perovskite solar cells, the second peak or shoulder at low frequency is of special interest. Several groups observed a peak at low frequencies and speculated that mobile ions could be the cause.[16,33] Our measurement shows a shoulder rather than a peak in a similar frequency range. The IMPS simulation reproduces this peak. We can therefore confirm the hypothesis that mobile ions are responsible for the low-frequency peak. The frequency of the peak depends on the ion mobility as shown in Figure 5c. Without mobile ions, the peak vanishes. To the best of our knowledge, this is the first published drift-diffusion simulation of IMPS including mobile ions.

We conclude that the three experiments in the frequency domain are well suited to study ion conductivity.

The plots in Figure 3 have been obtained using a manual fitting procedure as outlined in our previous publication.[21] Some parameters are assumed to be known (active area and layer thickness), and some are taken from literature (permittivity) or can be directly analyzed (series resistance). Starting with "realistic" parameters for mobilities, recombination efficiency, energy levels, and ion and trapping values, we then obtained initial results, which were manually fitted after "inspection by eye". For this, the criterion was that specific features like a rise or peak were reproduced at a correct timescale and magnitude. Tables 1 and 2 show the resulting material and device parameters obtained from the fit and used

Table 2. Layer-Independent Simulation Parameters Used for All Simulations in Figures 3−5

parameter	value
external series resistance	25 Ω (analysed)
device area	0.065 cm² (measured)
temperature	293 K (measured)
boundary condition top electrode hole-density	6.8×10^{18} 1/cm³
boundary condition bottom electrode electron-density	6.5×10^{17} 1/cm³

in all simulations shown in Figure 3. We want to stress again that the parameter set was identical for every simulation and only the operating condition that is characterization technique was varied.

We present a numerical device model for perovskite solar cells that is capable of describing consistently all major effects found in a variety of opto-electrical experiments. The electron and hole mobilities of the perovskite layer are 0.2 and 0.1 cm²/ V s, respectively. This is at the lower end of published mobilities for polycrystalline MAPI perovskites (0.1−25 cm²/ V s[37]). In our drift-diffusion model, the charge carrier mobility is an effective macroscopic quantity of the layer including grain boundaries. The low bulk mobility might be explained by the rather small crystals (~100 nm[26]) of our perovskite solar cells. The recombination coefficient of 1×10^{-10} cm³/s lies in the expected range (1×10^{-9} to 1×10^{-10} cm³/s[38]). The contact properties show ohmic injection in agreement with previous results on the same stack.[26] The trap depth of 0.5 eV was chosen according to results of Baumann et al. from thermally stimulated currents.[36]

3.1. Governing Physical Effects. When mobile ions accumulate at an interface with a transport layer (HTM or ETM), the charge injection property of this interface is altered, with applied voltage ions migrating from one interface toward the other. These two effects cause the JV curve hysteresis (Figure 3a−c), the high capacitance at low frequencies under illumination (Figure 3h), and the delayed current rise in the voltage pulse experiments (Figure 3f).

The simulation results of Figure 3 are very sensitive to the doping density of the boundary layers TaTm and C₆₀. If the contact layers are highly conductive, most of the potential drops are within the perovskite layer.[24] Ions compensate this voltage drop when they move to the interfaces. The JV curve hysteresis does therefore most probably also depend on the conductivity of the boundary layers. A high conductivity would lead to a higher potential drop inside the bulk and therefore to a more pronounced JV curve hysteresis.

In solar cells with small built-in fields, surface recombination plays an important role because the low electric field charges may reach the opposite contact and recombine there. A passivated contact can hinder such recombination. In our material system, the interface recombination is suppressed in a similar way as it is done in highly efficient organic LED stacks.[39] The addition of 10 nm of intrinsic transport layer material on both sides leads to an effectively suppressed surface recombination.[26] Omitting these thin intrinsic passivation layers alters the voltage step response as discussed in the Supporting Information. Our model results are consistent: decent agreement between simulation and measurement is only reached with a low surface recombination.

We have shown in a previous publication that even in the presence of mobile ions, the JV curve hysteresis vanishes if the surface recombination is sufficiently low and the diffusion length is sufficiently high.[40] In the present case, the contacts are passivated, minimizing surface recombination. The JV curve hysteresis observed at faster scan rates can therefore be related to a relatively short diffusion length leading to high bulk recombination of charge carriers. In the Supporting Information, we show that improving the bulk quality (lower SRH recombination and higher charge carrier mobility) reduces the hysteresis significantly.

The order of magnitude of the high capacitance under illumination is reproduced by the simulation. However, the simulation always shows a distinct capacitance plateau for low frequencies, while the measurements often show a steady rise. A possible explanation is dispersive ion motion. While in our model we assume a constant and homogeneous ion mobility, this may not hold in real perovskite layers where, for example, because of grain boundaries, ion transport may in fact be dispersive.[29] In a simple picture, a unique ion mobility gives rise to one characteristic frequency in the impedance (as well as IMPS) experiment, while a distribution of mobilities should lead to a "smeared-out" transition and therefore a continued rise of the capacitance.

3.2. Reverse Voltage Step. To complement the set of experiments shown in Figure 3, we perform an additional experiment: a voltage step from forward to reverse. Figure 6 shows the measurement and simulation of a voltage step from +3 to −3 V. In this case, the simulation fails to describe the measurement.
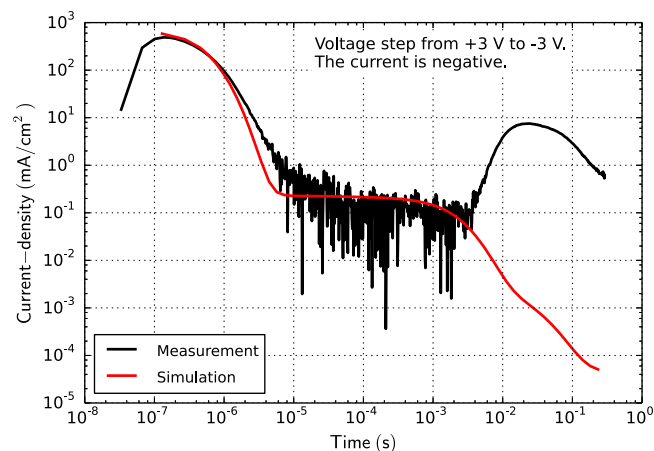
Figure 6. Measurement and simulation result of a MAPI perovskite solar cell. A voltage step to +3 V is applied for 300 ms. At t = 0, the voltage is changed to −3 V. The current response is shown. The simulation fails to describe the measured current.

In the measurement, a reverse current is observed starting at 3 ms and vanishing after 1 s. The simulated current shows a time-of-flight[41,42] behavior. The ions are preconditioned in the forward direction. Most of the iodine vacancies accumulate within the first nanometres close to the ETM interface. When the voltage is reversed, these ions migrate through the bulk until they reach the HTM interface. The ion movement leads to a drift current of around 0.2 mA/cm². When the interface is reached after the transit time of 3 ms, the current goes to zero in the simulation. At this point, the additional current peak, observed in the measurement, starts. The integrated current density results in a sheet charge density of 4.4×10^{13} cm⁻². If the assumed ion density of 5×10^{17} cm⁻³ is integrated over the
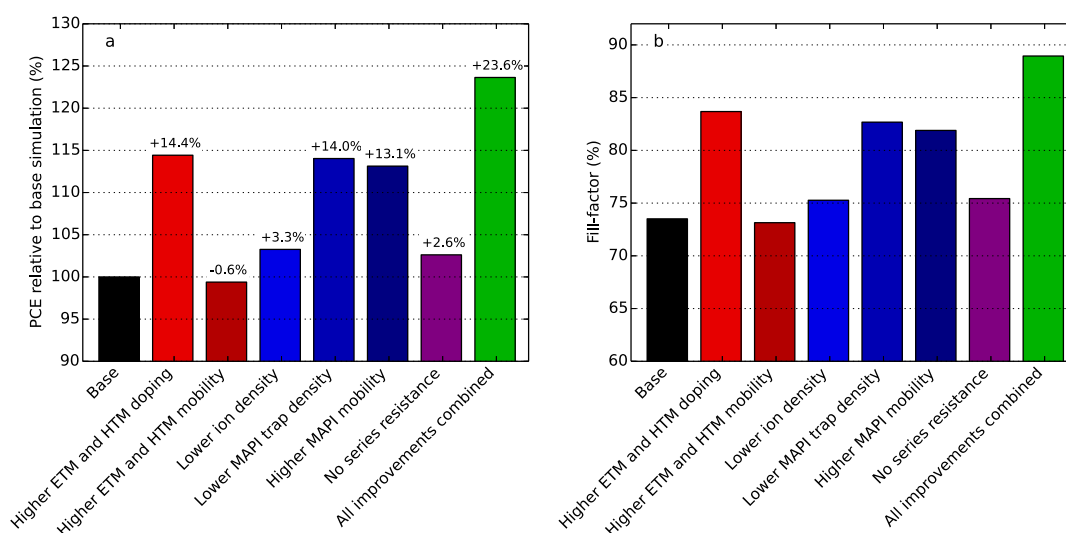
Figure 7. Parameter variation on the basis of the simulation results of Tables 1 and 2. (a) Power conversion efficiency improvement for different parameter variations. (b) Fill factor for different parameter variations.

MAPI thickness, a comparable sheet charge of 2.5×10^{13} cm^{-2} is obtained. We therefore speculate that a chemical reaction occurs at one of the interfaces leading to a reduction or oxidation of the contact material induced by the mobile ions. This effect does not occur in MAPI perovskite solar cells with TiO$_2$ and spiro-OMeTAD contact layers; therefore, it seems to be dependent on the choice of contact material. Alternatively, reverse injection may be responsible for this transient current. The effect deserves further investigation and the simulation model may need to be adapted accordingly.

3.3. Model Limitations. In this section, we discuss further possible model limitations.

- In the presented model, the interfaces between layers are sharp and the layers are homogeneous. The devices studied here show an interface roughness of about 10 nm.[26]

- In our model, two mobile ion species (positive and negative) are used. In reality, there may be more than two active species.[43,44] In the Supporting Information, we show that a model with only one mobile species and a second, immobile species produces very similar effects.

- We use constant mobilities for the migration of ions. In reality, ion migration may be field-dependent and dispersive. Furthermore, Shao et al. showed that ions migrate preferably along grain boundaries.[45] In such a case, two mobilities for the same ion type might be required for its description: a bulk ion mobility and an ion mobility along the grain boundaries.

- We do not impose an upper limit on the local ion concentration at the layer boundaries. This is a subject of our ongoing investigations and will be discussed elsewhere.

3.4. Parameter Study. On the basis of the simulation results, we perform steady-state JV curve simulations. This allows us to assess the influence of specific parameters on the power conversion efficiency. The power conversion efficiency and the fill-factor are shown in Figure 7.

A doping density of 10^{19} 1/cm^3 in both transport layers improves the charge carrier extraction at the contacts and leads to a higher fill factor. The resistive losses in the ETM and HTM do, however, not limit the performance. Using 10 times higher electron and hole mobilities does not improve the performance.

A smaller density of mobile ions (10% compared to the base simulation) leads only to a minor device improvement of 3.3%. The mobile ions are not a major obstacle for efficient device operation if the charge carrier mobility is high enough and the surface recombination is low enough.[40] Reducing the trap density to 10% of the base simulation leads to a large improvement by 14% due to reduced SRH-recombination. A similar improvement is reached for 10 times higher electron and hole mobilities in the perovskite material leading to better charge extraction. The external series resistance as caused by the lateral conductivity of the TCO can reduce the performance significantly.[46] Reducing it to zero leads to an improvement of only 2% in our case. With all the effects combined, a relative performance improvement of 23% is obtained. The improvement stems mainly from a higher fill factor (Figure 7b). Further performance improvements could be achieved by optimized light management.[2]

4. CONCLUSIONS

We performed a variety of characterization experiments with vacuum-deposited MAPI perovskite solar cells, including JV curves with different scan rates, light-intensity-dependent open-circuit voltage, impedance spectroscopy, IMPS, transient photocurrents, and transient voltage steps.

We developed a multilayer drift-diffusion simulation model incorporating mobile ions to simulate all experimental techniques. A decent agreement between simulation and measurement is reached for all techniques using only one parameter set in the simulation. To the best of our knowledge, this is the first study presenting a consistent device model that is capable of simultaneously describing transient, steady-state, and frequency-dependent experimental results of perovskite solar cells.

Our study shows that it is necessary to consider mobile ions and SRH recombination in the simulation to reproduce experimental results. Whether one, two, or even more different mobile ionic species are incorporated does not play a major role for reproducing the experimental results by simulation. Further model complexity like ferroelectricity or considering

individual grain boundaries is not required to understand and describe the device physics of perovskite cells.

As the physical processes in perovskite solar cells are complex, an approach combining different experimental techniques is required to achieve consistent, accurate, and reliable results. We show a possible path to reach this goal and discuss the limitations of this approach. Using the device model with the derived parameters allows us to study different approaches to improve the cell performance.

The delayed current peak resulting from a voltage step to a negative voltage can, however, not be reproduced with the drift-diffusion model. We speculate that either reverse injection or a reversible redox reaction of ions with the contact layer material may be responsible for this effect. Further effort is required to extend the device model accordingly.

■ ASSOCIATED CONTENT

Ⓢ Supporting Information

The Supporting Information is available free of charge on the ACS Publications website at DOI: 10.1021/acsami.9b04991.

> Physical model; model parameter analysis—simulation results with none, one or two mobile ion species; voltage pulse—influence of surface recombination; *IV*-curve hysteresis; and all measurement data (PDF)

■ AUTHOR INFORMATION

Corresponding Author

*E-mail: andreas.schiller@fluxim.com.

ORCID Ⓞ

Martin T. Neukom: 0000-0002-9454-3545

Michele Sessolo: 0000-0002-9189-3005

Henk J. Bolink: 0000-0001-9784-6253

Notes

The authors declare no competing financial interest.

■ REFERENCES

(1) Ramírez Quiroz, C. O.; Shen, Y.; Salvador, M.; Forberich, K.; Schrenker, N.; Spyropoulos, G. D.; Heumüller, T.; Wilkinson, B.; Kirchartz, T.; Spiecker, E.; et al. Balancing electrical and optical losses for efficient 4-terminal Si-perovskite solar cells with solution processed percolation electrodes. *J. Mater. Chem. A* **2018**, *6*, 3583−3592.

(2) Altazin, S.; Stepanova, L.; Werner, J.; Niesen, B.; Ballif, C.; Ruhstaller, B. Design of Perovskite/Crystalline-Silicon Monolithic Tandem Solar Cells. *Opt. Express* **2018**, *26*, A579.

(3) Filipič, M.; Löper, P.; Niesen, B.; De Wolf, S.; Krč, J.; Ballif, C.; Topič, M. CH_3NH_3PbI_3 Perovskite/Silicon Tandem Solar Cells: Characterization Based Optical Simulations. *Opt. Express* **2015**, *23*, A263.

(4) Snaith, H. J.; Abate, A.; Ball, J. M.; Eperon, G. E.; Leijtens, T.; Noel, N. K.; Stranks, S. D.; Wang, J. T.-W.; Wojciechowski, K.; Zhang, W. Anomalous Hysteresis in Perovskite Solar Cells. *J. Phys. Chem. Lett.* **2014**, *5*, 1511−1515.

(5) Juarez-Perez, E. J.; Sanchez, R. S.; Badia, L.; Garcia-Belmonte, G.; Kang, Y. S.; Mora-Sero, I.; Bisquert, J. Photoinduced Giant Dielectric Constant in Lead Halide Perovskite Solar Cells. *J. Phys. Chem. Lett.* **2014**, *5*, 2390−2394.

(6) Tress, W.; Marinova, N.; Moehl, T.; Zakeeruddin, S. M.; Nazeeruddin, M. K.; Grätzel, M. Understanding the Rate-Dependent J−V Hysteresis, Slow Time Component, and Aging in CH_3NH_3PbI_3 Perovskite Solar Cells: The Role of a Compensated Electric Field. *Energy Environ. Sci.* **2015**, *8*, 995−1004.

(7) Walsh, A.; Scanlon, D. O.; Chen, S.; Gong, X. G.; Wei, S.-H. Self-Regulation Mechanism for Charged Point Defects in Hybrid Halide Perovskites. *Angew. Chem., Int. Ed.* **2015**, *54*, 1791−1794.

(8) Eames, C.; Frost, J. M.; Barnes, P. R. F.; O'Regan, B. C.; Walsh, A.; Islam, M. S. Ionic Transport in Hybrid Lead Iodide Perovskite Solar Cells. *Nat. Commun.* **2015**, *6*, 7497.

(9) Lee, H.; Gaiaschi, S.; Chapon, P.; Marronnier, A.; Lee, H.; Vanel, J.-C.; Tondelier, D.; Bourée, J.-E.; Bonnassieux, Y.; Geffroy, B. Direct Experimental Evidence of Halide Ionic Migration under Bias in CH_3NH_3PbI_{3−x}Cl_x-Based Perovskite Solar Cells Using GD-OES Analysis. *ACS Energy Lett.* **2017**, *2*, 943−949.

(10) van Reenen, S.; Kemerink, M.; Snaith, H. J. Modeling Anomalous Hysteresis in Perovskite Solar Cells. *J. Phys. Chem. Lett.* **2015**, *6*, 3808−3814.

(11) Richardson, G.; O'Kane, S. E. J.; Niemann, R. G.; Peltola, T. A.; Foster, J. M.; Cameron, P. J.; Walker, A. B. Can slow-moving ions explain hysteresis in the current-voltage curves of perovskite solar cells? *Energy Environ. Sci.* **2016**, *9*, 1476−1485.

(12) Courtier, N. E.; Richardson, G.; Foster, J. M. A Fast and Robust Numerical Scheme for Solving Models of Charge Carrier Transport and Ion Vacancy Motion in Perovskite Solar Cells. *Appl. Math. Model.* **2018**, *63*, 329−348.

(13) Calado, P.; Telford, A. M.; Bryant, D.; Li, X.; Nelson, J.; O'Regan, B. C.; Barnes, P. R. F. Evidence for Ion Migration in Hybrid Perovskite Solar Cells with Minimal Hysteresis. *Nat. Commun.* **2016**, *7*, 13831.

(14) O'Kane, S. E. J.; Richardson, G.; Pockett, A.; Niemann, R. G.; Cave, J. M.; Sakai, N.; Eperon, G. E.; Snaith, H. J.; Foster, J. M.; Cameron, P. J.; et al. Measurement and Modelling of Dark Current Decay Transients in Perovskite Solar Cells. *J. Mater. Chem. C* **2017**, *5*, 452−462.

(15) Walter, D.; Fell, A.; Wu, Y.; Duong, T.; Barugkin, C.; Wu, N.; White, T.; Weber, K. Transient Photovoltage in Perovskite Solar Cells: Interaction of Trap-Mediated Recombination and Migration of Multiple Ionic Species. *J. Phys. Chem. C* **2018**, *122*, 11270−11281.

(16) Pockett, A.; Eperon, G. E.; Sakai, N.; Snaith, H. J.; Peter, L. M.; Cameron, P. J. Microseconds, Milliseconds and Seconds: Deconvoluting the Dynamic Behaviour of Planar Perovskite Solar Cells. *Phys. Chem. Chem. Phys.* **2017**, *19*, 5959−5970.

(17) Belisle, R. A.; Nguyen, W. H.; Bowring, A. R.; Calado, P.; Li, X.; Irvine, S. J. C.; McGehee, M. D.; Barnes, P. R. F.; O'Regan, B. C. Interpretation of Inverted Photocurrent Transients in Organic Lead Halide Perovskite Solar Cells: Proof of the Field Screening by Mobile Ions and Determination of the Space Charge Layer Widths. *Energy Environ. Sci.* **2017**, *10*, 192−204.

(18) Jacobs, D. A.; Shen, H.; Pfeffer, F.; Peng, J.; White, T. P.; Beck, F. J.; Catchpole, K. R. The Two Faces of Capacitance: New Interpretations for Electrical Impedance Measurements of Perovskite Solar Cells and Their Relation to Hysteresis. *J. Appl. Phys.* **2018**, *124*, 225702.

(19) *Semiconducting Thin Film Optics Simulator (SETFOS)*; Fluxim AG: Switzerland.

(20) Neukom, M. T.; Züfle, S.; Ruhstaller, B. Reliable Extraction of Organic Solar Cell Parameters by Combining Steady-State and Transient Techniques. *Org. Electron.* **2012**, *13*, 2910−2916.

(21) Neukom, M.; Züfle, S.; Jenatsch, S.; Ruhstaller, B. Opto-Electronic Characterization of Third-Generation Solar Cells. *Sci. Technol. Adv. Mater.* **2018**, *19*, 291−316.

(22) *Platform for All-in-One Characterization (PAIOS)*; Fluxim AG: Switzerland.

(23) Ershov, M.; Liu, H. C.; Li, L.; Buchanan, M.; Wasilewski, Z. R.; Jonscher, A. K. Negative Capacitance Effect in Semiconductor Devices. *IEEE Trans. Electron Devices* **1998**, *45*, 2196−2206.

(24) Tessler, N.; Vaynzof, Y. Preventing Hysteresis in Perovskite Solar Cells by Undoped Charge Blocking Layers. *ACS Appl. Energy Mater.* **2018**, *1*, 676−683.

(25) Courtier, N. E.; Cave, J. M.; Foster, J. M.; Walker, A. B.; Richardson, G. How Transport Layer Properties Affect Perovskite Solar Cell Performance: Insights from a Coupled Charge Transport/Ion Migration Model. *Energy Environ. Sci.* **2019**, *12*, 396−409.

(26) Momblona, C.; Gil-Escrig, L.; Bandiello, E.; Hutter, E. M.; Sessolo, M.; Lederer, K.; Blochwitz-Nimoth, J.; Bolink, H. J. Efficient Vacuum Deposited P-i-n and n-i-p Perovskite Solar Cells Employing Doped Charge Transport Layers. *Energy Environ. Sci.* **2016**, *9*, 3456−3463.

(27) Kirchartz, T.; Deledalle, F.; Tuladhar, P. S.; Durrant, J. R.; Nelson, J. On the Differences between Dark and Light Ideality Factor in Polymer:Fullerene Solar Cells. *J. Phys. Chem. Lett.* **2013**, *4*, 2371−2376.

(28) Kirchartz, T.; Nelson, J. Meaning of Reaction Orders in Polymer:Fullerene Solar Cells. *Phys. Rev. B: Condens. Matter Mater. Phys.* **2012**, *86*, 165201.

(29) Moia, D.; Gelmetti, I.; Calado, P.; Fisher, W.; Stringer, M.; Game, O.; Hu, Y.; Docampo, P.; Lidzey, D.; Palomares, E.; et al. Ionic-to-Electronic Current Amplification in Hybrid Perovskite Solar Cells: Ionically Gated Transistor-Interface Circuit Model Explains Hysteresis and Impedance of Mixed Conducting Devices. *Energy Environ. Sci.* **2019**, *12*, 1296−1308.

(30) Ebadi, F.; Taghavinia, N.; Mohammadpour, R.; Hagfeldt, A.; Tress, W. Origin of Apparent Light-Enhanced and Negative Capacitance in Perovskite Solar Cells. *Nat. Commun.* **2019**, *10*, 1574.

(31) Byers, J. C.; Ballantyne, S.; Rodionov, K.; Mann, A.; Semenikhin, O. A. Mechanism of Recombination Losses in Bulk Heterojunction P3HT:PCBM Solar Cells Studied Using Intensity Modulated Photocurrent Spectroscopy. *ACS Appl. Mater. Interfaces* **2011**, *3*, 392−401.

(32) Li, J.; Peter, L. M. Surface Recombination at Semiconductor Electrodes: Part III. Steady-State and Intensity Modulated Photocurrent Response. *J. Electroanal. Chem. Interfacial Electrochem.* **1985**, *193*, 27−47.

(33) Correa-Baena, J.-P.; Anaya, M.; Lozano, G.; Tress, W.; Domanski, K.; Saliba, M.; Matsui, T.; Jacobsson, T. J.; Calvo, M. E.; Abate, A.; et al. Unbroken Perovskite: Interplay of Morphology, Electro-Optical Properties, and Ionic Movement. *Adv. Mater.* **2016**, *28*, 5031−5037.

(34) Sherkar, T. S.; Momblona, C.; Gil-Escrig, L.; Ávila, J.; Sessolo, M.; Bolink, H. J.; Koster, L. J. A. Recombination in Perovskite Solar Cells: Significance of Grain Boundaries, Interface Traps, and Defect Ions. *ACS Energy Lett.* **2017**, *2*, 1214−1222.

(35) Wilson, J. N.; Frost, J. M.; Wallace, S. K.; Walsh, A. Perspective: Dielectric and Ferroic Properties of Halide Perovskite Solar Cells. **2018**, arXiv:1811.01832 Cond-Mat.

(36) Baumann, A.; Väth, S.; Rieder, P.; Heiber, M. C.; Tvingstedt, K.; Dyakonov, V. Identification of Trap States in Perovskite Solar Cells. *J. Phys. Chem. Lett.* **2015**, *6*, 2350−2354.

(37) Levine, I.; Gupta, S.; Bera, A.; Ceratti, D.; Hodes, G.; Cahen, D.; Guo, D.; Savenije, T. J.; Ávila, J.; Bolink, H. J.; et al. Can We Use Time-Resolved Measurements to Get Steady-State Transport Data for Halide Perovskites? *J. Appl. Phys.* **2018**, *124*, 103103.

(38) Paulke, A.; Stranks, S. D.; Kniepert, J.; Kurpiers, J.; Wolff, C. M.; Schön, N.; Snaith, H. J.; Brenner, T. J. K.; Neher, D. Charge Carrier Recombination Dynamics in Perovskite and Polymer Solar Cells. *Appl. Phys. Lett.* **2016**, *108*, 113505.

(39) Lee, J.; Chen, H.-F.; Batagoda, T.; Coburn, C.; Djurovich, P. I.; Thompson, M. E.; Forrest, S. R. Deep Blue Phosphorescent Organic Light-Emitting Diodes with Very High Brightness and Efficiency. *Nat. Mater.* **2016**, *15*, 92−98.

(40) Neukom, M. T.; Züfle, S.; Knapp, E.; Makha, M.; Hany, R.; Ruhstaller, B. Why Perovskite Solar Cells with High Efficiency Show Small IV-Curve Hysteresis. *Sol. Energy Mater. Sol. Cells* **2017**, *169*, 159−166.

(41) Clarke, T. M.; Peet, J.; Nattestad, A.; Drolet, N.; Dennler, G.; Lungenschmied, C.; Leclerc, M.; Mozer, A. J. Charge Carrier Mobility, Bimolecular Recombination and Trapping in Polycarbazole Copolymer:Fullerene (PCDTBT:PCBM) Bulk Heterojunction Solar Cells. *Org. Electron.* **2012**, *13*, 2639−2646.

(42) Chan, K. K. H.; Tsang, S. W.; Lee, H. K. H.; So, F.; So, S. K. Charge Injection and Transport Studies of Poly(2,7-Carbazole) Copolymer PCDTBT and Their Relationship to Solar Cell Performance. *Org. Electron.* **2012**, *13*, 850−855.

(43) Li, Z.; Xiao, C.; Yang, Y.; Harvey, S. P.; Kim, D. H.; Christians, J. A.; Yang, M.; Schulz, P.; Nanayakkara, S. U.; Jiang, C.-S.; et al. Extrinsic Ion Migration in Perovskite Solar Cells. *Energy Environ. Sci.* **2017**, *10*, 1234−1242.

(44) Domanski, K.; Correa-Baena, J.-P.; Mine, N.; Nazeeruddin, M. K.; Abate, A.; Saliba, M.; Tress, W.; Hagfeldt, A.; Grätzel, M. Not All That Glitters Is Gold: Metal-Migration-Induced Degradation in Perovskite Solar Cells. *ACS Nano* **2016**, *10*, 6306−6314.

(45) Shao, Y.; Fang, Y.; Li, T.; Wang, Q.; Dong, Q.; Deng, Y.; Yuan, Y.; Wei, H.; Wang, M.; Gruverman, A.; et al. Grain Boundary Dominated Ion Migration in Polycrystalline Organic−Inorganic Halide Perovskite Films. *Energy Environ. Sci.* **2016**, *9*, 1752−1759.

(46) Neukom, M. T.; Reinke, N. A.; Ruhstaller, B. Charge Extraction with Linearly Increasing Voltage: A Numerical Model for Parameter Extraction. *Sol. Energy* **2011**, *85*, 1250−1256.

(47) Hunter, J. D. Matplotlib: A 2D Graphics Environment. *Comput. Sci. Eng.* **2007**, *9*, 90−95.